aerospace

MDPI

Article

Model Predictive Control-Based Attitude Control of Under-Actuated Spacecraft Using Solar Radiation Pressure

Lei Jin * and Yingjie Li

School of Astronautics, Beihang University, 37 Xueyuan Road, Beijing 100191, China
* Correspondence: jinleibuaa@163.com

Abstract: An attitude control strategy for an under-actuated spacecraft with two reaction wheels is proposed, using the active assistance of solar radiation pressure torque. By changing the rotation angles of the solar panels, the magnitude and direction of the solar radiation pressure torque is assumed to be adjustable in this paper. The attitude dynamic model of a rigid spacecraft with two reaction wheels and two solar panels is established and transformed into the form of a non-linear system. An integrated control scheme based on dual-mode model predictive control is proposed, which obtains the rotation speeds of the solar panels and the rotation accelerations of the reaction wheels directly as control quantities. Using this control method, not only are the constraints of rotation speeds and rotation angles of the panels satisfied, but also the robustness of the closed-loop system is ensured. The simulation results prove the validity of the proposed control method.

Keywords: under-actuated spacecraft; solar radiation pressure; attitude control; model predictive control

check for updates

Citation: Jin, L.; Li, Y. Model Predictive Control-Based Attitude Control of Under-Actuated Spacecraft Using Solar Radiation Pressure. *Aerospace* **2022**, *9*, 498. https://doi.org/10.3390/aerospace9090498

Academic Editor: Weizong Wang

Received: 29 July 2022
Accepted: 2 September 2022
Published: 7 September 2022

1. Introduction

Reaction wheels (RWs) are often used as the main attitude control actuators of spacecraft, especially the small satellites and deep space probes. Due to the constraints of weight and cost, the three or four RWs configuration without back-up is often applied [1,2]. However, after working on the orbit for a long time, some of the RWs will inevitably fail, and the attitude control system of spacecraft may be degraded to be under-actuated [3], such as the Far Ultraviolet Spectroscopic Explorer (FUSE) [4,5] and the BIRD satellite [6]. In this case, the attitude control performance of spacecraft will decline, which even leads to the failure to complete the scheduled task. Therefore, the research on the attitude control of under-actuated spacecraft is of great significance to improve the control performance and prolong the life of spacecraft.

In the research on the attitude control of under-actuated spacecraft using two RWs, most of the existing studies are obtained under the assumption of the conservation of system angular momentum [7–14]. However, environmental torque really exists for the spacecraft, which means the system angular momentum cannot be conserved and the existing studies cannot obtain good control results in engineering application. Environmental torque is usually treated as a disturbance in the design of the spacecraft attitude control system. Therefore, a small number of scholars have studied the attitude control of underactuated spacecraft when the environmental torque is regarded as the disturbance. However, the research results show that this will greatly increase the difficulty and complexity of the design of the under-actuated attitude controller [15,16], which is also not suitable for engineering practice. In fact, from the early stage of spacecraft development, there have been examples of using environmental torque to realize spacecraft active/passive control [17–19]. Because it has the advantages of zero energy consumption, high reliability and low cost, it is particularly attractive for small satellites and deep space detectors.

Based on the above research ideas, there have been a few studies using environmental torque as an aid to jointly realize the three-axis attitude control of under-actuated spacecraft. For low-orbiting spacecraft, Zeng [20] uses the aerodynamic torque generated by the pneumatic rudder to control the attitude of the satellite's pitch axis and uses the flywheel to control the attitude of the rolling yaw axis. Forbes et al. [21], Angelis et al. [22] and Ousaloo [23] used the geomagnetic environmental torque generated by magnetic torquer and two/one flywheels to jointly realize the spacecraft attitude stabilization. Keshtkar et al. [24] proposed and applied a sliding mode approach-based control algorithm to an under-actuated mechanical system, which consists of two control moment gyros for the triaxial attitude control of a gravity-gradient stabilized tethered satellite system. For high-orbiting spacecraft, the main environmental torque is the solar radiation pressure (SRP) which cannot be ignored. Lee studied the stable control of the pitch axis of the spacecraft by using only the solar pressure torque [25,26]. The Kepler telescope lost two out of its four RWs before its mission was completed, and the small thrusters and SRP torque were used to assist the attitude control [27]. A recent study [28] introduced SRP torque into the model of the under-actuated spacecraft with RWs and achieved a certain degree of attitude stability by the passive SRP torque assistance under the assumption of linearization. However, the magnitude and direction of the SRP torque cannot be adjusted actively, which restricts the engineering application of this method.

In recent decades, a new type of spacecraft—the solar sail spacecraft that relies on the pressure of sunlight to create a propulsive force on the sail membrane—has been widely discussed in deep space exploration. The torque of solar sail can be actively controlled by changing the centroid distance [29], the illuminated area [30] and the reflectivity [31] of the solar panel.

Inspired by the research idea of using the adjustable torque of solar sail for solar sail spacecraft control, combined with the fact that most solar panels installed on spacecraft have one or two rotational degrees of freedom, we innovatively propose that the magnitude and direction of the SRP torque can be actively controlled by adjusting the rotation angles or speeds of the solar panels, so that the three-axis attitude control of under-actuated spacecraft using two RWs can be realized with the assistance of SRP torque.

Based on the above analysis, a new attitude control strategy of under-actuated spacecraft with the active assistance of SRP torque is proposed in this paper. Firstly, the attitude dynamic model of a rigid spacecraft bus with two RWs and two solar panels is established, in which the SRP torque model is also obtained. Secondly, the dynamic and kinematic models are transformed into the form of a non-linear system, in which the rotation speeds of the solar panels and the rotation accelerations of the RWs are directly set as control inputs. Thirdly, the dual-mode Model Predictive Control (MPC) method is used to design the controller. Finally, the simulation results illustrate the validity of this control strategy.

The main innovative contributions of this paper are listed as follows.

Firstly, for under-actuated spacecraft, especially those operating in high orbit, we propose that the SRP torque can be actively adjusted and used to assist the reaction wheels, so as to ensure the complete three-axis torque output and restore the three-axis attitude control of spacecraft. In particular, by actively adjusting the rotation speeds of the solar panels, the magnitude and direction of the SRP can be actively controlled, so as to further improve the attitude control performance and prolong the working life of the spacecraft.

Secondly, an integrated control scheme based on dual-mode MPC is proposed. Instead of setting control torques as inputs, the rotation speeds of the solar panels and the rotation accelerations of the RWs are directly obtained as control inputs, which simplifies the controller design steps. More importantly, based on the MPC method, the rotation angles and speeds of the solar panels are constrained within a certain range, so as to ensure that the normal direction of the panel is as close to the sun as possible in the control process, and the flexible vibration of solar panels will not be excited easily. Therefore, the proposed control method has better engineering applicability.

This paper is organized as follows. In Section 2, the attitude kinematic equation based on Euler angles, and the attitude dynamic equation of a rigid spacecraft with two RWs and two solar panels are established. In Section 3, the system model is transformed into a generalized nonlinear system and the dual-mode MPC method is used to design the controller for the system. In Section 4, the validity of the proposed method is verified. Finally, the conclusions are summarized in Section 5.

2. Spacecraft Model

2.1. Kinematics and Dynamics of Spacecraft

In order to make the control strategy proposed in this paper more applicable, we assume that the spacecraft runs along the heliocentric orbit. The spacecraft structure and the related coordinate systems are defined as shown in Figure 1. The coordinate frame that is fixedly attached to the spacecraft body is represented by $S_b(O_bX_bY_bZ_b)$. O_b lies on the center of the mass of the satellite bus. The orbital coordinate frame is defined as $S_o(O_oX_oY_oZ_o)$ with the Z_o axis always pointing to the sun, the X_o axis aligned along the spacecraft motion direction, and the Y_o axis satisfying the right-handed frame. The panel coordinate frames are, respectively, defined as $S_{a1}(O_{a1}X_{a1}Y_{a1}Z_{a1})$ and $S_{a2}(O_{a2}X_{a2}Y_{a2}Z_{a2})$. O_{a1} and O_{a2} are on the middle of the hinges between the solar panels and the driving mechanism. Y_{a1} and Y_{a2} are set as the rotation axes of the panels and aligned with the body axis Y_b. Z_{a1} and Z_{a2} are perpendicular to the surfaces of the panels and aligned with the body axis Z_b at the zero position, as shown in Figure 1.

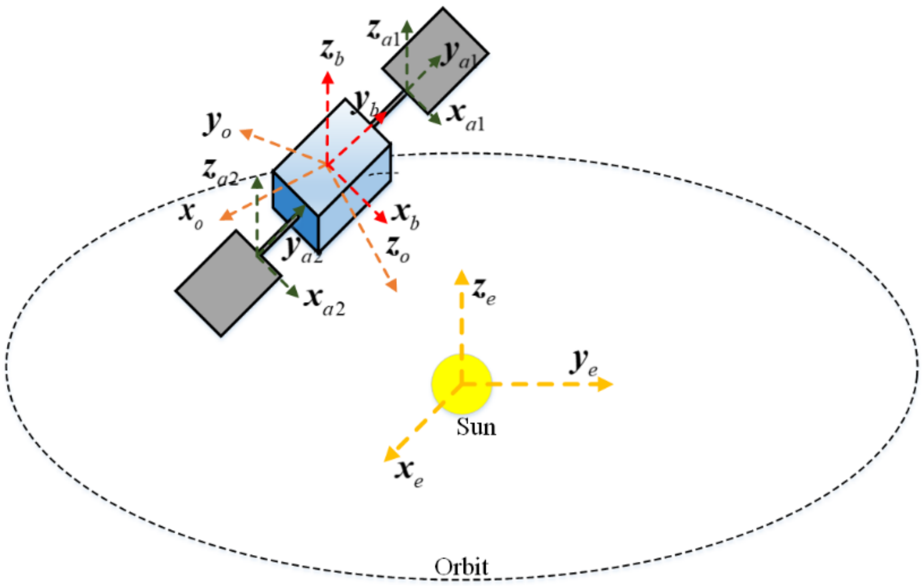

Figure 1. Cuboid spacecraft schematic with two solar panels.

The rotation angles of the solar panels relative to the zero position are defined as β_1 and β_2.The orientation of the frame S_b with respect to the frame S_o is specified by Euler angles (roll φ, pitch θ, and yaw ψ) with a 3-1-2 sequence. The spacecraft attitude kinematics can be expressed as

$$\boldsymbol{\omega}_b = \boldsymbol{L}_y(\theta)\boldsymbol{L}_x(\varphi)\boldsymbol{L}_z(\psi)\begin{bmatrix}0\\0\\\dot{\psi}\end{bmatrix} + \boldsymbol{L}_y(\theta)\boldsymbol{L}_x(\varphi)\begin{bmatrix}\dot{\varphi}\\0\\0\end{bmatrix} + \boldsymbol{L}_y(\theta)\begin{bmatrix}0\\\dot{\theta}\\0\end{bmatrix} + \boldsymbol{L}_{bo}\begin{bmatrix}0\\-\omega_o\\0\end{bmatrix} \tag{1}$$

where $\boldsymbol{\omega}_b$ represents the absolute angular velocity vector of the spacecraft expressed in the frame S_b, ω_o represents the orbital angular velocity, and $\boldsymbol{L}_y(\theta), \boldsymbol{L}_x(\varphi), \boldsymbol{L}_z(\psi)$ represent the attitude conversion matrices, respectively. The spacecraft attitude kinematics can be rearranged into the following form

$$\boldsymbol{\omega}_b = \boldsymbol{J}_{vb}\dot{\boldsymbol{\theta}}_b - \boldsymbol{J}_{wo}\omega_o \tag{2}$$

where $\dot{\boldsymbol{\theta}}_b = \begin{bmatrix} \dot{\varphi} & \dot{\theta} & \dot{\psi} \end{bmatrix}^{\boldsymbol{T}}$ represents Euler angular velocity array, and $\boldsymbol{J}_{vb}$ and $\boldsymbol{J}_{wo}$ can be written as

$$\boldsymbol{J}_{vb} = \begin{bmatrix} \cos\theta & 0 & -\cos\varphi\sin\theta \\ 0 & 1 & \sin\varphi \\ \sin\theta & 0 & \cos\varphi\cos\theta \end{bmatrix}, \boldsymbol{J}_{wo} = \begin{bmatrix} \sin\psi\cos\theta + \sin\varphi\sin\theta\cos\psi \\ \cos\psi\cos\varphi \\ \sin\psi\sin\theta - \sin\varphi\cos\theta\cos\psi \end{bmatrix} \tag{3}$$

The dynamic model of a rigid spacecraft with flexible attachments has been derived in many research papers. The rotation equation of the central rigid body with two RWs and two solar panels, and the rotation equation and vibration equation of the solar panels can be expressed as [32]

$$\boldsymbol{I_T}\dot{\boldsymbol{\omega}}_b + \sum_{k=1}^{2} \boldsymbol{R}_{bak}\dot{\boldsymbol{\omega}}_{ak} + \sum_{k=1}^{2} \boldsymbol{F}_{bak}\ddot{\boldsymbol{\eta}}_{ak} + \boldsymbol{\omega}_b^*(\boldsymbol{I_t}\boldsymbol{\omega}_b + \boldsymbol{C}\boldsymbol{I}_w\boldsymbol{\Omega}) = \boldsymbol{T_r} + \boldsymbol{T}_{srp} + \boldsymbol{T}_d \tag{4}$$

$$\boldsymbol{I}_{ak}\dot{\boldsymbol{\omega}}_{ak} + \boldsymbol{F}_{ak}\ddot{\boldsymbol{\eta}}_{ak} + \boldsymbol{R}_{bak}^{\boldsymbol{T}}\dot{\boldsymbol{\omega}}_b = \boldsymbol{T}_{ak}, (k = 1, 2) \tag{5}$$

$$\ddot{\boldsymbol{\eta}}_{ak} + 2\xi_{ak}\boldsymbol{\Lambda}_{ak}\dot{\boldsymbol{\eta}}_{ak} + \boldsymbol{\Lambda}_{ak}^2\boldsymbol{\eta}_{ak} + \boldsymbol{F}_{bak}^{\boldsymbol{T}}\dot{\boldsymbol{\omega}}_b = 0, (k = 1, 2) \tag{6}$$

In Equation (4), $\boldsymbol{I_t}$ is the total inertia matrix of the system consisting of spacecraft body, RWs and solar panels, which can be expressed as

$$\boldsymbol{I_t} = \boldsymbol{I}_b + \boldsymbol{C}\boldsymbol{I}_w\boldsymbol{C}^{\boldsymbol{T}} + \sum_{j=1}^{2} m_j\left(\boldsymbol{r}_j^{\boldsymbol{T}}\boldsymbol{r}_j\boldsymbol{I}_3 - \boldsymbol{r}_j\boldsymbol{r}_j^{\boldsymbol{T}}\right) + \sum_{k=1}^{2} \boldsymbol{I}_{bak} \tag{7}$$

where $\boldsymbol{I}_b$ is the sum of central rigid body inertia and lateral inertias of RWs; $\boldsymbol{I_w}$ represents the diagonal matrix consisting of the same rotational inertia of RWs as I_w; $\boldsymbol{C}$ represents the installation matrix of RWs; m_j is the mass of the jth RW; and $\boldsymbol{r}_j$ is the position vector of the mass center of the jth RW with respect to $S_b(O_bX_bY_bZ_b)$. $\boldsymbol{I}_{bak}$ is the inertia of the kth solar panel with respect to $S_b(O_bX_bY_bZ_b)$, expressed as $\boldsymbol{I}_{bak} = \boldsymbol{C}_{bak}\boldsymbol{I}_{ak}\boldsymbol{C}_{bak}^{\boldsymbol{T}} + m_{ak}\boldsymbol{L}_{ak}$, where $\boldsymbol{C}_{bak}$ is the convert matrix from the panel coordinate frame of the kth solar panel to the body coordinate system $S_b(O_bX_bY_bZ_b)$; $\boldsymbol{I}_{ak}$ is the inertia of the kth solar panel with respect to $S_{ak}(O_{ak}X_{ak}Y_{ak}Z_{ak}), k = 1, 2$; m_{ak} is the mass of the kth solar panel; and $\boldsymbol{L}_{ak}$ can be calculated by the vector $\boldsymbol{r}_{bak} = \begin{bmatrix} x_k & y_k & z_k \end{bmatrix}, k = 1, 2$, which denotes the position of the origin of the kth panel coordinate frames in the spacecraft body frame and is expressed as

$$\boldsymbol{L}_{ak} = \begin{bmatrix} y_k^2 + z_k^2 & -x_ky_k & -x_kz_k \\ -x_ky_k & x_k^2 + z_k^2 & -y_kz_k \\ -x_kz_k & -y_kz_k & x_k^2 + y_k^2 \end{bmatrix}, k = 1, 2$$

The definition of the new symbols in Equations (4)–(6) are as follows: $\boldsymbol{\Omega}$ represents the RWs speed vector; $\boldsymbol{T_r} = -\boldsymbol{C}\boldsymbol{I}_w\dot{\boldsymbol{\Omega}}$ is the output torque of the RWs; $\boldsymbol{T}_{srp}$ is the SRP torque; $\boldsymbol{T_d}$ is the unknown disturbance torque; $\boldsymbol{T}_{ak}$ represents the external torque acting on the solar panel; $\boldsymbol{\omega}_{ak}$ is the angular velocity of solar panels with respect to the rigid spacecraft; $\boldsymbol{\eta}_{ak}$ is the normalized modal coordinates; $\boldsymbol{\Lambda}_{ak}$ is the modal frequency diagonal matrix of the solar panel; ξ_{ak} represents the modal damping matrix of the solar panel; $\boldsymbol{R}_{bak}$ is the rigid coupling coefficient matrix of the rotation of solar panel acting on the rotation of the central rigid body; $\boldsymbol{F}_{bak}$ represents the flexible coupling coefficient matrix of the vibration of the solar panel acting on the rotation of a central rigid body; and $\boldsymbol{F}_{ak}$ is the flexible coupling coefficient matrix of the vibration of solar panel acting on its own rotation. $\boldsymbol{\omega}_b^*$ is an anti-symmetric matrix shown as

$$\boldsymbol{\omega}_b^* = \begin{bmatrix} 0 & -\omega_{bz} & \omega_{by} \\ \omega_{bz} & 0 & -\omega_{bx} \\ -\omega_{by} & \omega_{bx} & 0 \end{bmatrix}$$

where ω_{bx}, ω_{by} and ω_{bz} are the three elements of $\boldsymbol{\omega}_b$.

Remark 1. *The control method proposed in Section 3 is more suitable for the spacecraft in heliocentric orbit. Heliocentric orbit has two advantages. One is the long lighting time, which means that the SRP torque can be used for most of the time during the orbit; the other is that the SRP torque is the main environmental torque for the spacecraft and the magnitude is large enough so that it can be used for the attitude control of spacecraft. Although the selection of the heliocentric orbit leads to the narrowing of the application scope of the proposed control method, the control strategy in this paper still has important engineering application value for the heliocentric orbit spacecraft when the fault actuator cannot be repaired and replaced.*

Remark 2. *Reaction wheels such as the four skew type and the three orthogonal plus one skew type are widely used as the attitude control actuators of the spacecrafts. However, for the long-life spacecrafts, especially the deep space probes, one or several reaction wheels may have faults or even break down after working for a long time. In this case, the spacecraft may be degraded to the underactuated spacecraft. Therefore, in this section, the attitude dynamic model of the spacecraft with two reaction wheels is established, which stands for the typical case.*

Remark 3. *From Equation (4), it can be seen that the rotation and vibration of solar panels will result in disturbances on the attitude control of the central rigid body. In addition, the system inertia varies with the rotation of the solar panels. We will discuss how to deal with the disturbances and the inertia variation in the section of control law design.*

2.2. The Model of Solar Radiation Pressure Torque

To model the SRP torque acting on the spacecraft, we assume that the rigid spacecraft is a homogeneous hexahedron. The two solar panels are installed along the Y_b axis, and the initial orientation of the panels is set to ensure the normal direction of the solar panels pointing to the sun. The solar panels are controlled by electromotor rotation around the Y_b axis, and their rotation angles are defined as $\beta_j, j = 1, 2$.

The force $d\vec{F}$ acting on the area element dA due to the solar radiation pressure can be expressed as follows [33]:

$$d\vec{F} = -P\cos(\gamma)\left\{(\rho_a + \rho_d)\vec{s} + \left[2\rho_s\cos(\gamma) + \frac{2}{3}\rho_d\right]\vec{n}\right\}dA \tag{8}$$

where P is the constant solar pressure, dA is the area element illuminated by the sun, $\vec{s}$ is the unit sun direction vector, $\vec{n}$ is the unit external normal direction vector of the area element, γ is the angle between the above two vectors, and ρ_s, ρ_{a}, $\rho_{\boldsymbol{t}}$ and ρ_d, respectively, stand for the specular reflectivity, the absorptivity, the index of refraction and the diffuse reflectance, satisfying $\rho_s + \rho_{\mathrm{a}} + \rho_{\boldsymbol{t}} + \rho_d = 1$.

As mentioned before, the rigid spacecraft is assumed to be a homogeneous hexahedron, no shadows will emerge, as the spacecraft is always facing the sun in its nominal attitude motion. Therefore, the total SRP torque acting on the six facets of the rigid spacecraft can be expressed as

$$\vec{T}_{b\_srp} = \sum_{i=1,\cdots 6} \vec{r}_i \times d\vec{F}_i \tag{9}$$

where $\vec{r}_i (i = 1, \ldots, 6)$ represents the distance vector from the center of mass of the spacecraft to the geometric center of the ith facet of the rigid spacecraft, and $d\vec{F}_i (i = 1, \ldots, 6)$ represents the SRP force acting on the ith facet of the rigid spacecraft. As the mass center of the spacecraft body is close to its own centroid, $\vec{r}_i$ and the normal direction vector of the ith facet of the rigid spacecraft are almost in the same direction. In this case, $\vec{T}_{b\_srp}$ almost equals to zero and can be neglected in the controller design. However, the real $\vec{T}_{b\_srp}$ will be added as a kind of disturbance torque in the simulation.

As is known to all, the thickness of most of the solar panels is small. Therefore, by ignoring the SRP torque acting on the sides of the solar panels, the SRP torque acting on the upper and lower surfaces of the solar panels can be expressed as

$$\vec{T}_{s\_srp} = -\sum_{j=1,2} PA_j \vec{r}_j \times \left\{ (\rho_a + \rho_d) \left| \vec{s} \cdot \vec{n}_j \right| \vec{s} + 2\rho_s \left(\vec{s} \cdot \vec{n}_j \right) \left| \vec{s} \cdot \vec{n}_j \right| \vec{n}_j + \frac{2}{3}\rho_d \left(\vec{s} \cdot \vec{n}_j \right) \vec{n}_j \right\} \tag{10}$$

where A_j is the area of the solar panel, $\vec{n}_j$ is the unit normal direction vector of the solar panels, and $\vec{r}_j$ is the vector from the center of mass of the spacecraft to the geometric center of the solar panel, satisfying $\left|\vec{r}_1\right| = \left|\vec{r}_2\right|$. Finally, we can obtain the components of the SRP torque expressed in frame S_b as

$$\begin{gathered} T_{srpx} = \sum_{j=1,2} -PA_j r_j \{ (\rho_a + \rho_d) |\cos\varphi| \left|\cos(\theta + \beta_j)\right| \cos\varphi \cos\theta \\ +2\rho_s |\cos\varphi| \left|\cos(\theta + \beta_j)\right| \cos\varphi \cos(\theta + \beta_j) \cos\beta_j + \frac{2}{3}\rho_d \cos\varphi \cos(\theta + \beta_j) \cos\beta_j \} \end{gathered} \tag{11}$$

$$T_{srpy} = 0 \tag{12}$$

$$\begin{gathered} T_{srpz} = \sum_{j=1,2} -PA_j r_j \{ (\rho_a + \rho_d) |\cos\varphi| \left|\cos(\theta + \beta_j)\right| \cos\varphi \sin\theta \\ -2\rho_s |\cos\varphi| \left|\cos(\theta + \beta_j)\right| \cos\varphi \cos(\theta + \beta_j) \sin\beta_j - \frac{2}{3}\rho_d \cos\varphi \cos(\theta + \beta_j) \sin\beta_j \} \end{gathered} \tag{13}$$

Remark 4. *The installation of the solar panels relative to the rigid spacecraft used in this paper determines that the SRP torque can be provided along the rolling axis and yaw axis of the spacecraft body.*

Remark 5. *The following SRP assisted control method is proposed based on the assumption that the residual reaction wheels and SRP can still provide the full three-axis torque after the failure of the reaction wheels. Therefore, whether the proposed control strategy in the next part is feasible or not depends on the location of the failure reaction wheels and the installation configuration of the solar panels. For example, as the SRP torque is zero along the Y_b axis according to the installation configuration of solar panels in this paper, there is still no torque to provide along the Y_b axis if the Y_b axis reaction wheel fails.*

Remark 6. *The existence of planets near the spacecraft was ignored in our discussion, so the influence of the albedo of other planets on the control scheme design was not discussed. However, if it is assumed that there are other planets near the spacecraft with a certain albedo, the solar array will receive not only the light from the sun, but also the light reflected from other planets. At this time, the two parts of the SPR torque on the panels can be modeled separately, and then the control scheme can be designed reasonably according to the magnitude and direction of the two parts of SPR torque and the different lighting conditions. It can be predicted that the control scheme will be more complicated when the planetary albedo is considered, but the total SPR torque amplitude may increase, which is beneficial to the control.*

3. Control Law Design

The control object in this paper is to achieve the attitude stabilization of the underactuated spacecraft with two RWs, by rotating the solar panel angles to provide the assistant SRP torque. Therefore, a suitable control law needs to be designed to obtain the commanded rotation speeds of the RWs and the solar panels. However, the rotation and vibration of the solar panels have certain interference in the attitude control of the spacecraft. If the rotation speeds of the solar panels are too fast, it will excite the severe flexible vibration of the solar panel, which may reduce the attitude control precision or even make the attitude control system of the spacecraft unstable. Therefore, the constraint of the rotation speeds of the solar panels must be taken into account in control law design. In addition, the angles of solar panels must be limited to a certain range in order to ensure the photoelectric conversion efficiency of solar panels.

Considering the nonlinearity of the system model and the constraints discussed above, it is almost impossible to obtain the exact analytical solutions of the control variables directly. A model predictive control-based control strategy is designed to resolve the control problem proposed in this paper. The essence of MPC is to solve the constrained open-loop optimal control problem in a finite time domain repeatedly. For a constrained nonlinear system, the optimization problem is transformed into solving the corresponding Hamilton–Jacobi–Bellman (HJB) equation, and MPC can express the constraints explicitly in the optimization problem at every moment. In addition, MPC has closed-loop stability and robustness due to rolling optimization.

Taking the angles and the rotation speeds of the solar panels as the state and control variables of the overall system, respectively, we can design the MPC. Firstly, MPC is developed on the basis of terminal inequality constraints to converge the state variables in the predictive time domain to the terminal domain. Secondly, a dual mode switching control scheme using MPC control outside the terminal domain and local linear control law in the terminal domain is proposed.

3.1. Control Scheme Based on Dual Mode MPC

In order to obtain the suitable spacecraft model for the control law design, we made the following assumptions: (1) The rotation speeds of the solar panels will be constrained, so the effect of the rotation and vibration of the solar panels on the attitude control of spacecraft is small, which can be neglected in the control law design. However, in the follow-up simulation, it will be added as the disturbance to test the validity and performance of the designed controller. (2) The inertias of RWs and solar panels is far less than the inertia of the central rigid body and can be ignored. In addition, we assume that the body frame S_b is a principal axis coordinate frame. Then we can have $\boldsymbol{I_t} \approx \boldsymbol{I}_b = diag\begin{pmatrix} I_x & I_y & I_z \end{pmatrix}^T$ as a constant diagonal matrix, which can simplify the control law design. However, the original expression of the system inertia matrix as Equation (7) will be used in the simulation to illustrate the robustness of the control law regarding the inertia error. (3) SRP torque is the main environmental torque for the spacecraft and $\boldsymbol{T_d}$ can be neglected in the control law design. However, in the simulation, $\boldsymbol{T_d}$ will be added to test the robustness of the designed controller. (4) In this paper, we assume that the two RWs are installed along the Y_b and Z_b axis, respectively. Then, the following simplified rigid body rotational dynamic equation can be obtained from Equation (4) as

$$\boldsymbol{I}_b\dot{\boldsymbol{\omega}}_b + \boldsymbol{\omega}_b^{\times}(\boldsymbol{I}_b\boldsymbol{\omega}_b + \boldsymbol{h}) = \boldsymbol{T}_r + \boldsymbol{T}_{srp} \tag{14}$$

where $\boldsymbol{h} = \boldsymbol{C}\boldsymbol{I}_w\boldsymbol{\Omega} = \begin{bmatrix} 0 & h_y & h_z \end{bmatrix}^T$.

Since the control object is to achieve the attitude stabilization in the orbital reference frame, it can be assumed that the attitude angles and angular velocities of the spacecraft are small quantities. Therefore, the kinematic equation as Equation (1) can be simplified as follows

$$\boldsymbol{\omega}_b = \begin{bmatrix} \dot{\varphi} - \omega_o\psi \\ \dot{\theta} - \omega_o \\ \dot{\psi} + \omega_o\varphi \end{bmatrix} \tag{15}$$

Then, we substitute Equation (12) and the time derivative of Equation (15) into Equation (14), and the following affine nonlinear system state equation can be obtained

$$\dot{\boldsymbol{x}} = \boldsymbol{f}(\boldsymbol{x}) + \boldsymbol{B}\boldsymbol{u} \tag{16}$$

where $\boldsymbol{x}$ is the extended state variable given by:

$$\boldsymbol{x} = \begin{bmatrix} \varphi & \theta & \psi & \dot{\varphi} & \dot{\theta} & \dot{\psi} & \beta_1 & \beta_2 \end{bmatrix}^T \tag{17}$$

the control signals can be chosen as:

$$\boldsymbol{u} = \begin{bmatrix} \dot{\beta}_1 & \dot{\beta}_2 & \dot{\Omega}_1 & \dot{\Omega}_2 \end{bmatrix}^T \tag{18}$$

where $\begin{bmatrix} \dot{\beta}_1 & \dot{\beta}_2 \end{bmatrix}^T$ are the rotation speeds of the solar panels, and $\begin{bmatrix} \dot{\Omega}_1 & \dot{\Omega}_2 \end{bmatrix}^T$ are the angular accelerations of the RWs. The expressions of the nonlinear term and the control coefficient matrix in Equation (16) are as follows

$$\boldsymbol{f}(\boldsymbol{x}) = \begin{bmatrix} \dot{\varphi} \\ \dot{\theta} \\ \dot{\psi} \\ \dfrac{-\omega_o(I_y - I_x - I_z)\dot{\psi} - \omega_o{}^2(I_y - I_z)\varphi + h_z\omega_o + T_{srpx}(\boldsymbol{x})}{I_x} \\ 0 \\ \dfrac{-\omega_o(I_x - I_y + I_z)\dot{\varphi} - \omega_o{}^2(I_y - I_x)\psi + T_{srpz}(\boldsymbol{x})}{I_z} \\ 0 \\ 0 \end{bmatrix} \tag{19}$$

$$\boldsymbol{B} = \begin{bmatrix} & & \mathbf{0}_{4\times 4} & \\ 0 & 0 & -\dfrac{I_w}{I_y} & 0 \\ 0 & 0 & 0 & -\dfrac{I_w}{I_z} \\ 1 & 0 & 0 & 0 \\ 0 & 1 & 0 & 0 \end{bmatrix} \tag{20}$$

It should be noted that in Equation (19), the expressions of SRP torque are shown in Equations (11) and (13) and are not linearized. As the SPR torque is the main research object of this paper, the more accurate modeling of the SPR torque and its application to control can verify the feasibility of this control algorithm.

As the rotation speeds of the solar panels are regarded as the control variables of the system equation, the unstable effect caused by the rotation and vibration of the solar panels can be reduced by applying constraints on the control variables.

Then, the classical fourth order Runge–Kutta method is applied to obtain the system discrete prediction model of Equation (16) as

$$\begin{cases} \boldsymbol{x}_{n+1} = \boldsymbol{x}_n + \dfrac{h}{6}(\boldsymbol{k}_1 + 2\boldsymbol{k}_2 + 2\boldsymbol{k}_3 + \boldsymbol{k}_4) \\ \boldsymbol{k}_1 = \boldsymbol{f}(x_n) + \boldsymbol{B}\boldsymbol{u} \\ \boldsymbol{k}_2 = \boldsymbol{f}(x_n + 0.5h\boldsymbol{k}_1) + \boldsymbol{B}\boldsymbol{u} \\ \boldsymbol{k}_3 = \boldsymbol{f}(x_n + 0.5h\boldsymbol{k}_2) + \boldsymbol{B}\boldsymbol{u} \\ \boldsymbol{k}_4 = \boldsymbol{f}(x_n + h\boldsymbol{k}_3) + \boldsymbol{B}\boldsymbol{u} \end{cases} \tag{21}$$

where $\boldsymbol{x}_n$ and $\boldsymbol{x}_{n+1}$ represent the state variables at the moment of n and $n+1$, and h represents the sampling step of the discrete system.

Then, we need to set the constraints of the system state and control variables. As the control object is to achieve the attitude stabilization in the orbital frame, Euler angles are suitable for the control problem considered and the required stabilization attitude is far from the singularity. However, in order to avoid a numerical calculation problem when the attitude is close to the singular point, some boundary values for Euler angles should be established as

$$\varphi \in \left(-\frac{\pi}{2},\frac{\pi}{2}\right)\mathrm{rad}, \theta \in (-\pi,\pi]\mathrm{rad}, \psi \in (-\pi,\pi]\,\mathrm{rad} \tag{22}$$

During the entire attitude stabilization process, the angular velocity of the spacecraft is set to be in a small range as

$$\dot{\varphi},\dot{\theta},\dot{\psi} \in \left[-\frac{\pi}{45},\frac{\pi}{45}\right]\mathrm{rad/s} \tag{23}$$

In order to satisfy the suitable photoelectric conversion efficiency, we can restrict the angles of incidence of the sunlight on the panels by limiting the rotation angles of the solar panels within the following range as

$$\beta_1,\beta_2 \in \left[-\frac{\pi}{4},\frac{\pi}{4}\right]\mathrm{rad} \tag{24}$$

To avoid the bad effect of the large rotation speeds of the solar panels on the attitude control, we limit the rotation speeds of the solar panels within the following range as

$$\dot{\beta}_1,\dot{\beta}_2 \in \left[-\frac{\pi}{180},\frac{\pi}{180}\right]\mathrm{rad/s} \tag{25}$$

Similarly, the rotation accelerations of RWs need to be constrained as

$$\dot{\Omega}_1,\dot{\Omega}_2 \in [-20,20]\mathrm{rad/s^2} \tag{26}$$

In summary, the constraints set for the state variables of the system can be expressed as

$$\boldsymbol{x}(k) \in \boldsymbol{X}, \boldsymbol{X} = \{\boldsymbol{x} \in R^n | \boldsymbol{x} \in [\boldsymbol{x}_{\min},\boldsymbol{x}_{\max}]\}\ , k > 0 \tag{27}$$

where

$$\boldsymbol{x}_{\min} = \left[-\frac{\pi}{2},-\pi,-\pi,-\frac{\pi}{45},-\frac{\pi}{45},-\frac{\pi}{45},-\frac{\pi}{4},-\frac{\pi}{4}\right]^T$$
$$\boldsymbol{x}_{\max} = \left[\frac{\pi}{2},\pi,\pi,\frac{\pi}{45},\frac{\pi}{45},\frac{\pi}{45},\frac{\pi}{4},\frac{\pi}{4}\right]^T$$

The constraints set for the control variables of the system can be expressed as

$$\boldsymbol{u}(k) \in \boldsymbol{U}, \boldsymbol{U} = \{\boldsymbol{u} \in R^m | \boldsymbol{u} \in [\boldsymbol{u}_{\min},\boldsymbol{u}_{\max}]\}\ , k > 0 \tag{28}$$

where $\boldsymbol{u}_{\min} = \left[-\frac{\pi}{180},-\frac{\pi}{180},-20,-20\right]^T$, $\boldsymbol{u}_{\max} = \left[\frac{\pi}{180},\frac{\pi}{180},20,20\right]^T$.

After we obtain the explicit expression of the constraints, we can step into the most important part of control law design based on dual mode MPC, where we will calculate the terminal penalty matrix $\boldsymbol{P} \in R^{n\times n}$ and the terminal region $\Omega = \{\boldsymbol{x} \in \boldsymbol{R}^n | \boldsymbol{x}^T\boldsymbol{P}\boldsymbol{x} \le \alpha\}$ off-line, according to the off-line algorithm [34].

Algorithm:

(1) We assume that a linear controller to reach the local stabilization exists for the nonlinear system as Equation (16). Then, we set the equilibrium point as $\boldsymbol{x} = \boldsymbol{0}$ and Equation (16) can be linearized into the Jacobian linearization model as

$$\dot{\boldsymbol{x}} = \boldsymbol{A}\boldsymbol{x} + \boldsymbol{B}\boldsymbol{u} \tag{29}$$

where $\boldsymbol{A}$ is a Jacobian matrix expressed as $\boldsymbol{A} = \left.\frac{\partial f(\boldsymbol{x})}{\partial \boldsymbol{x}}\right|_{\boldsymbol{x}=0}$. For the linear system Equation (29), we can design a linear controller as

$$\boldsymbol{u} = \boldsymbol{K}\boldsymbol{x} \tag{30}$$

in which $\boldsymbol{K}$ is a constant gain matrix.

Then, the dynamic system becomes a typical second order system

$$\dot{\boldsymbol{x}} = \boldsymbol{A}_k \boldsymbol{x} \tag{31}$$

where $\boldsymbol{A}_k = \boldsymbol{A} + \boldsymbol{B}\boldsymbol{K}$ is also a constant matrix. Therefore, by designing the suitable feedback gain $\boldsymbol{K}$, the system can be asymptotically stable.

(2) The unique positive definite symmetric solution $\boldsymbol{P}$ can be obtained by solving the following discrete Lyapunov equation

$$\boldsymbol{A}_k^T \boldsymbol{P} \boldsymbol{A}_k - \boldsymbol{P} + \kappa \boldsymbol{Q}^* = 0 \tag{32}$$

where $\kappa > 1$, $\boldsymbol{Q}^*$ is expressed as

$$\boldsymbol{Q}^* = \boldsymbol{Q} + \boldsymbol{K}^T \boldsymbol{R} \boldsymbol{K} \in \boldsymbol{R}^{n \times n} \tag{33}$$

where $\boldsymbol{Q} \in \boldsymbol{R}^{n \times n}$ and $\boldsymbol{R} \in \boldsymbol{R}^{m \times m}$, respectively, denote the weight parameter matrices of the state variables $\boldsymbol{x}$ and the control variables $\boldsymbol{u}$, and can be adjusted according to the control objective.

(3) Look for $\alpha_1 > 0$ as large as possible so that for all the state variables $\boldsymbol{x}$ in the terminal domain, $\Omega_1 \in \boldsymbol{X}$ and $\boldsymbol{K}\boldsymbol{x} \in \boldsymbol{U}$ is satisfied. $\boldsymbol{X}$ and $\boldsymbol{U}$ are the constraints sets for the state variables $\boldsymbol{x}$ and the control variables $\boldsymbol{u}$ of the system as expressed in Equations (27) and (28).

$$\Omega_1 = \left\{ \boldsymbol{x} \in \boldsymbol{R}^n \middle| \boldsymbol{x}^T \boldsymbol{P} \boldsymbol{x} \le \alpha_1 \right\} \tag{34}$$

(4) We search for the largest $\alpha \in (0, \alpha_1]$ so that the following Hamilton–Jacobian–Bellman (HJB) inequality can be satisfied locally in $\Omega = \left\{ \boldsymbol{x} \in \boldsymbol{R}^n \middle| \boldsymbol{x}^t \boldsymbol{P} \boldsymbol{x} \le \alpha \right\}$.

$$V(\boldsymbol{x}(k+1)) - V(\boldsymbol{x}(k)) \le -\boldsymbol{x}^T(k) \boldsymbol{Q}^* \boldsymbol{x}(k) \tag{35}$$

where $V(\boldsymbol{x}(k)) = \boldsymbol{x}^T(k) \boldsymbol{P} \boldsymbol{x}(k)$.

Based on the above algorithm, we can obtain the terminal penalty matrix $\boldsymbol{P} \in R^{n \times n}$ and the terminal domain $\Omega = \left\{ \boldsymbol{x} \in \boldsymbol{R}^n \middle| \boldsymbol{x}^T \boldsymbol{P} \boldsymbol{x} \le \alpha \right\}$.

Then, we can describe the optimization problem for each sampling moment k as

$$\min_{\overline{u}(\cdot)} J(\boldsymbol{x}(k)) \tag{36}$$

with

$$J(\boldsymbol{x}(k)) = \sum_{i=0}^{N-1} \left(\|\boldsymbol{x}(k+i|k)\|_{\boldsymbol{Q}}^2 + \|\boldsymbol{u}(k+i|k)\|_{\boldsymbol{R}}^2 \right) + \|\boldsymbol{x}(k+N|k)\|_{\boldsymbol{P}}^2 \tag{37}$$

subject to

$$\boldsymbol{x}(k+i+1|k) = f(\boldsymbol{x}(k+i|k), \boldsymbol{u}(k+i|k)), \ \ \boldsymbol{x}(k|k) = \boldsymbol{x}(k) \tag{38}$$

$$\boldsymbol{x}(k+i) \in \boldsymbol{X}, \quad \forall i = 0, 1, \ldots N-1 \tag{39}$$

$$\boldsymbol{u}(k+i) \in \boldsymbol{U}, \quad \forall i = 0, 1, \ldots N-1 \tag{40}$$

$$\boldsymbol{x}(k+N) \in \Omega \tag{41}$$

where N is the prediction time domain. We solve the optimization problem and use the first term of the control sequence as the control input outside the terminal domain, so the dual-mode MPC control law can be written as:

$$
\boldsymbol{u}^*(k) = \begin{cases} \boldsymbol{u}^*(k|k), \boldsymbol{x} \notin \Omega \\ \boldsymbol{K}\boldsymbol{x}(k), \boldsymbol{x} \in \Omega \end{cases} \tag{42}
$$

Remark 7. *In this paper, we assume that all the system state variables $\boldsymbol{x}$ are measurable, but our main task is to design the control law. Therefore, we assume that the state variables can be measured accurately and ignore the measurement model. Although ignoring the noise and delay of the state measurement will change the accuracy and stability of the attitude control in the numerical simulation to a certain extent, it will not change the feasibility and effectiveness of the scheme of using the SPR torque to assist the control.*

3.2. Feasibility and Stability Analysis

For general affine nonlinear systems, the precondition for the implementation of the dual-mode MPC control scheme is that the linear model for the system's equilibrium is asymptotically stable in the terminal domain. If the initial states of the system are outside the terminal domain, it is necessary to prove that it can be driven into the terminal domain in a limited time. According to the rolling optimization principle of MPC, it is necessary to update the open-loop optimization problem with the latest measurements at each sampling time and solve it repeatedly. Therefore, it is required that the optimization problem is feasible at each sampling time, which means that at least one (unnecessary optimal) control function exists to satisfy the trajectory starting from the measurement state, while satisfying the state constraints and terminal non-optimal.

Under equality constraints, a theorem is given that proves that the optimization problem expressed as Equation (36) is feasible at every moment [35]; another theorem is given that proves that the optimal value of the objective function as Equation (36) at each sampling time will not increase [35]. The above two theorems show that if the initial states of the system are outside the terminal domain, the system states will finally be driven into the terminal domain in a limited time using the proposed MPC control law. Combined with the stability analysis of the linear controller as Equation (30), it can be seen that the whole system is closed-loop stable.

4. Simulation Results

In this section, numerical simulation experiments are carried out to illustrate the validity of the proposed SRP torque assisted attitude control strategy for the underactuated spacecraft.

First, the simulation parameters are given. The spacecraft operates on the heliocentric orbit with the distance of an astronomical unit away from the sun, and mainly consists of a central rigid body and two symmetrically installed solar panels. The inertia matrix of the central rigid body is

$$
\boldsymbol{I}_b = \begin{bmatrix} 0.02 & 0 & 0 \\ 0 & 0.058 & 0 \\ 0 & 0 & 0.0625 \end{bmatrix} \text{kg m}^2
$$

The mass of the kth solar panel is chosen as $m_{ak} = 0.08$ kg, and the inertia matrices of the two solar panels relative to the panel coordinate frames are

$$
\boldsymbol{I}_{a1} = 1 \times 10^{-3} \begin{bmatrix} 2.2223048 & -0.77296377 & 0 \\ -0.77296377 & 0.37285813 & 0 \\ 0 & 0 & 2.951629 \end{bmatrix} \text{kg m}^2
$$

$$
\boldsymbol{I}_{a2} = 1 \times 10^{-3} \begin{bmatrix} 2.2223048 & 0.77296377 & 0 \\ 0.77296377 & 0.37285813 & 0 \\ 0 & 0 & 2.951629 \end{bmatrix} \text{kg m}^2
$$

The size of the central body of the spacecraft is $50 \times 25 \times 20\ \text{cm}^3$, and the sizes of the two solar panels are the same as $80 \times 25 \times 1\ \text{cm}^3$. The coordinates of the attachment points of the two solar panels expressed in S_b are $\begin{bmatrix} 0 & 21 & 0 \end{bmatrix}^{\boldsymbol{T}}$cm and $\begin{bmatrix} 0 & -21 & 0 \end{bmatrix}^{\boldsymbol{T}}$cm, respectively, and the distances from the mass center of the central body to the geometric center of solar panels are the same as $\left|\vec{r}_1\right| = \left|\vec{r}_2\right| = 0.61$ m. The surface material characteristic parameters of the solar panels are chosen as $\rho_a = 0.75$, $\rho_d = 0$, and $\rho_s = 0.25$. The constant solar pressure P is set as $P = 4.5598 \times 10^{-6}\ \text{N}/\text{m}^2$.

The attitude control actuators are three-orthogonal plus one skew type RWs with the installation matrix

$$C = \begin{bmatrix} 1 & 0 & 0 & 1/\sqrt{3} \\ 0 & 1 & 0 & 1/\sqrt{3} \\ 0 & 0 & 1 & 1/\sqrt{3} \end{bmatrix}$$

We assume that the reaction wheels installed along the Y_b and Z_b axis are in the normal operation mode, while the other two RWs are in the failure mode with zero rotation speeds. The initial speeds of the normal RWs are $\boldsymbol{\Omega}_0 = \begin{bmatrix} 0 & 0 \end{bmatrix}^T$ rpm, and the moment of inertia of each RW about its spin axis is $I_w = 1 \times 10^{-5}\ \text{kg} \cdot \text{m}^2$.

In the simulation, the disturbance torque $\boldsymbol{T}_d$ can be approximately estimated according to the inertia of the spacecraft and the orbit altitude as follows

$$\boldsymbol{T}_d = 1 \times 10^{-9} \times \begin{cases} 0.8 + 1.1\sin(\omega_o t) + 1.2\sin(2\omega_o t) \\ \;\;1.2 + \sin(\omega_o t) + 0.9\sin(2\omega_o t) \quad \text{Nm} \\ \;1 + 0.8\sin(\omega_o t) + 1.1\sin(2\omega_o t) \end{cases}$$

As the proposed controller is designed based on the linearized kinematic model as Equation (15), in order to ensure the validity of the controller, we choose the initial attitudes and attitude velocities which are close to the stabilization in the simulation. The initial attitude angles of the spacecraft are $\boldsymbol{\theta}_0 = \begin{bmatrix} -8^\circ & 10^\circ & 9^\circ \end{bmatrix}^T$, and the initial angular velocities are $\dot{\boldsymbol{\theta}}_0 = \begin{bmatrix} 1.5^\circ/\text{s} & 1.5^\circ/\text{s} & 1.5^\circ/\text{s} \end{bmatrix}^T$. In the control scheme of dual-mode MPC, the weighting matrices in the objective function are $\boldsymbol{Q} = diag\left(1\ 1\ 1\ 1 \times 10^4\ 1\ 1\ 1 \times 10^{-6}\ 1 \times 10^{-6}\right)$ and $\boldsymbol{R} = diag\left(10^{-3}\ 10^{-3}\ 10^{-6}\ 10^{-6}\right)$. The forecast time domain and the control time domain are set as $N = 5$ and $M = 2$, respectively.

The proposed control strategy is first applied to perform three-axis stabilization control, and the simulation results are shown in Figures 2–9.

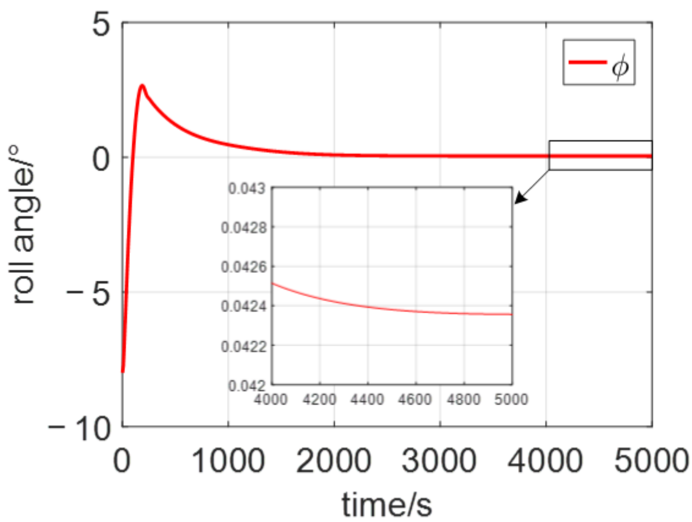

Figure 2. The time response of roll angle.

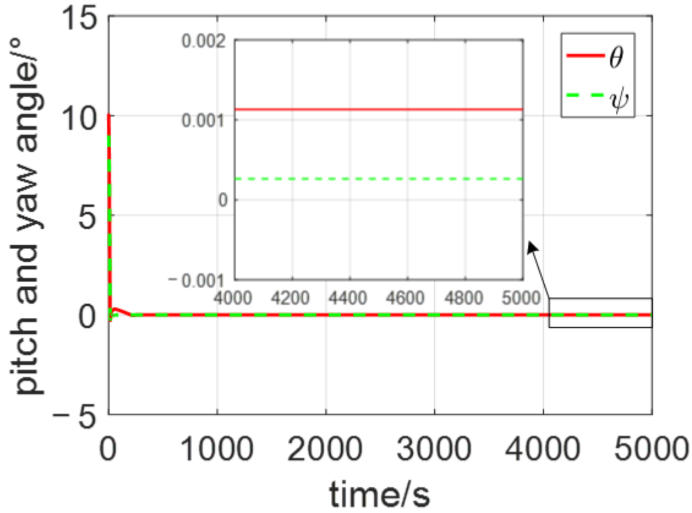

Figure 3. The time response of pitch and yaw angles.

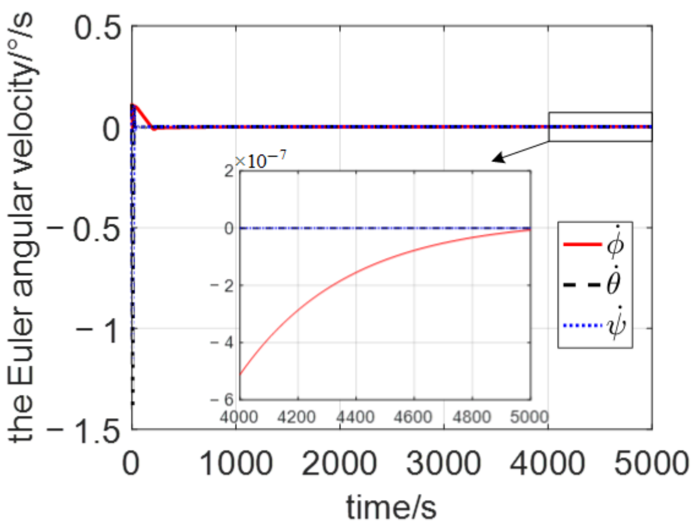

Figure 4. The time response of attitude angular velocities.

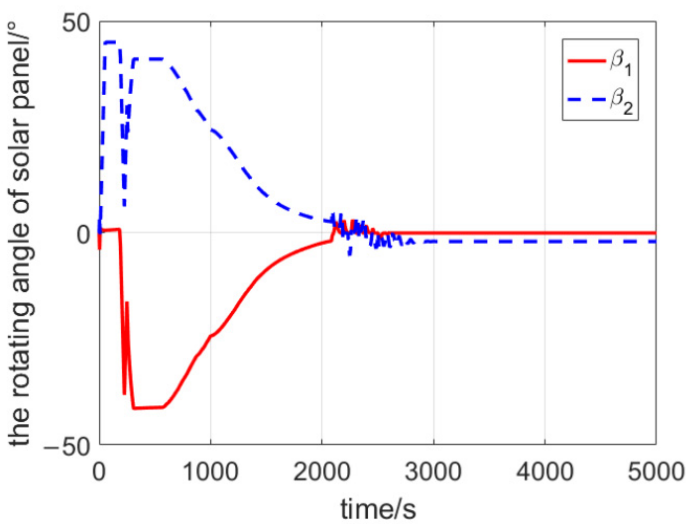

Figure 5. The time response of rotation angles of solar panels.

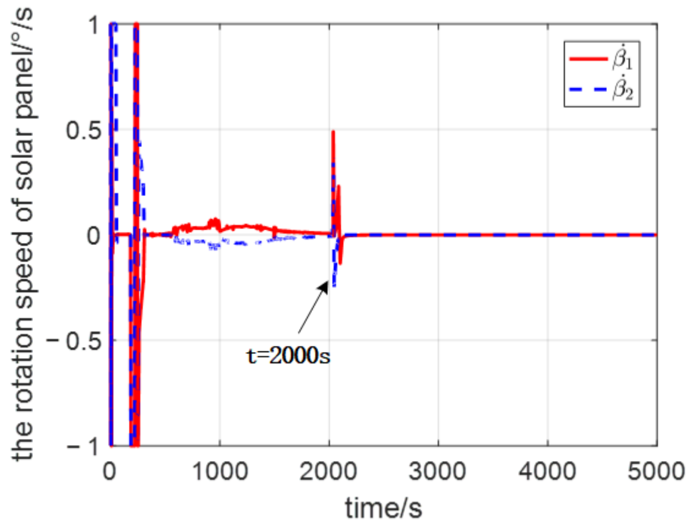

Figure 6. The time response of rotation speeds of solar panels.

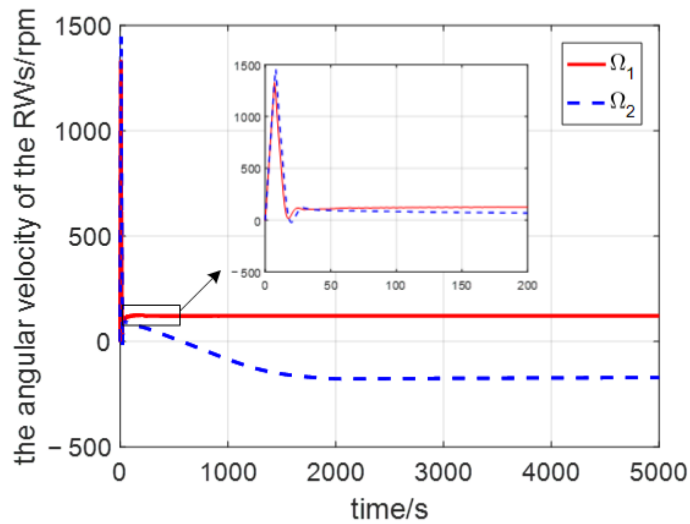

Figure 7. The time response of the angular velocity of RWs.

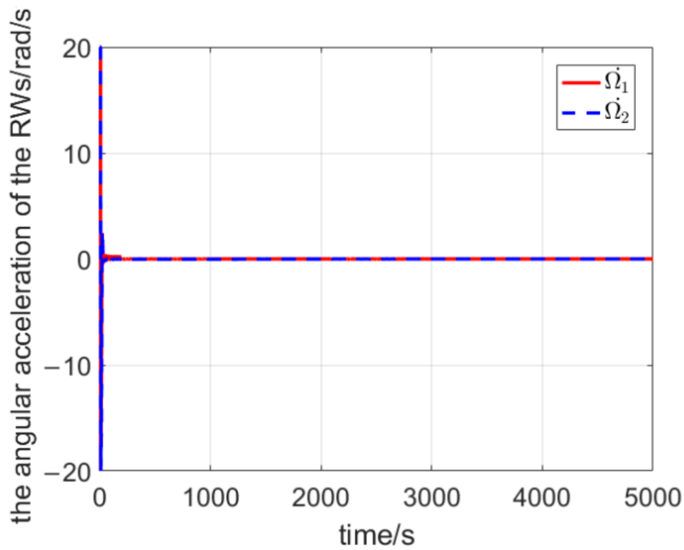

Figure 8. The time response of the angular acceleration of RWs.

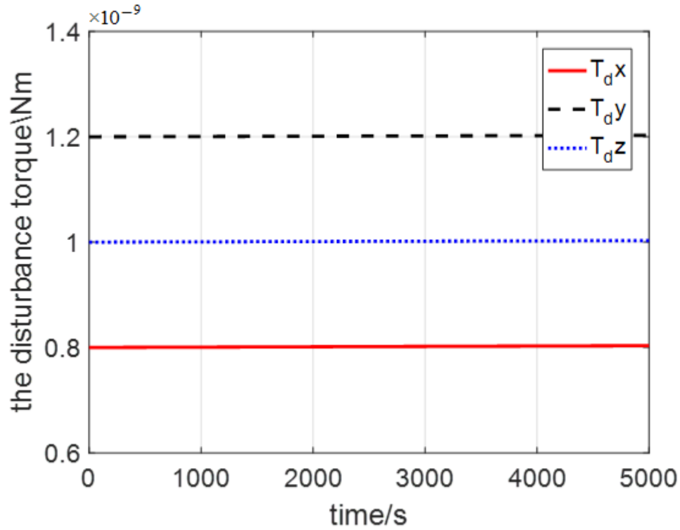

Figure 9. The time response of the disturbance torque.

According to Figures 2–4, the three-axis attitude angles and attitude angular velocities of the under-actuated spacecraft can be gradually stabilized using the dual-mode MPC controller, which proves the validity of the active assistance of the SRP torque. As the SRP torque is much smaller than the control torque provided by the RWs, we can see clearly that the convergence speed of the angular velocity and the attitude angle along the under-actuated axis is much slower than the other two axes. During the whole control course, the MPC control law is applied for the first 2000 s. At the moment of about the 2000th second, the system state is already near the equilibrium point, and the local linear control law is used since then. As there exists a switching of control laws, it can be seen that there is a sudden change for the amplitude of the rotation speeds of the solar panels at the moment of switching, as shown in Figure 6.

Figures 5–8 show the rotation angles and rotation speeds of solar panels, and the angular velocities and accelerations of RWs. It can be seen that the rotation angles and rotation speeds of solar panels and angular accelerations of RWs are all within the constraints we have specified, which shows that the dual-mode MPC has great advantages in handling constraints and has a high engineering application value. Figure 9 shows the external interference torque in the process.

Since the sun direction vector is always $\begin{bmatrix} 0 & 0 & 1 \end{bmatrix}^T$ in the orbit system, the angle between the normal vector of the panel and the sun direction vector is the smallest when the panel is at the zero position. Figure 5 shows that the rotation angles of panels finally keep within three degrees, which can ensure that there is enough power acquisition from the sun.

For the spacecraft working normally in space, the three-axis stabilization mode of the attitude control system may be switched to the single-axis pointing stabilization mode to perform space tasks, such as astronomical observation. In this case, the attitude control strategy proposed in this paper can also be used to achieve pointing stabilization. Here, we assume that the Z_b axis needs to point to the sun all the time. As the spacecraft operates on the heliocentric orbit with the distance of an astronomical unit away from the sun, the coordinate of the sun direction vector in the orbital coordinate system is always $\begin{bmatrix} 0 & 0 & 1 \end{bmatrix}^T$. Therefore, in order to achieve pointing stabilization, the Z_b axis should be controlled to align with the Z_o axis, which means that only the roll angle and pitch angle with respect to the orbital frame need to be stabilized, while the yaw angle does not need to be controlled. For the simulation, we change the weighting matrices in the objective function as $\boldsymbol{Q} = diag(1 \;\; 1 \;\; 0 \;\; 1\times10^4 \;\; 1 \;\; 0 \;\; 1\times10^{-6} \;\; 1\times10^{-6})$ and $\boldsymbol{R} = diag(10^{-3}\; 10^{-3}\; 10^{-6}\; 10^{-6})$, and the simulation results are shown in Figures 10–17.

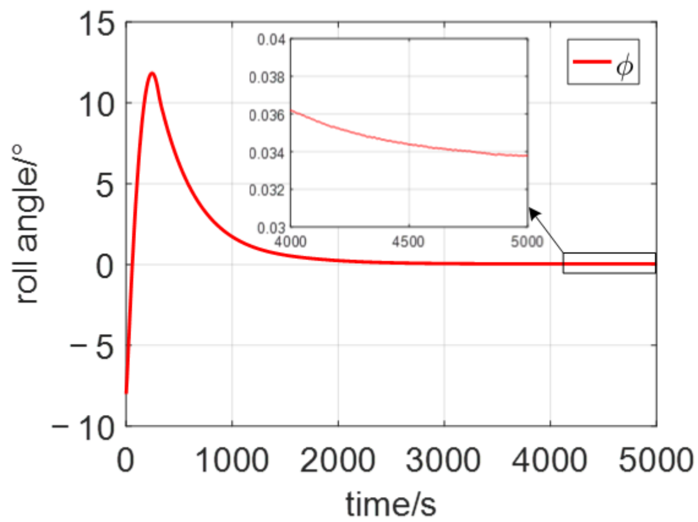

Figure 10. The time response of roll angle.

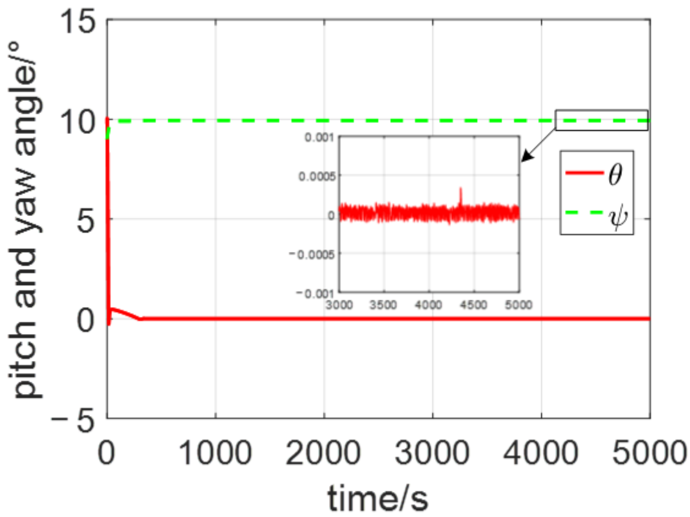

Figure 11. The time response of pitch and yaw angles.

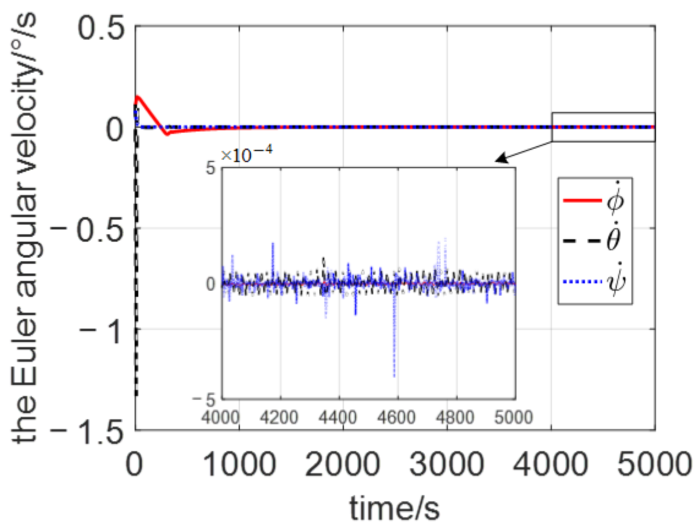

Figure 12. The time response of attitude angular velocities.

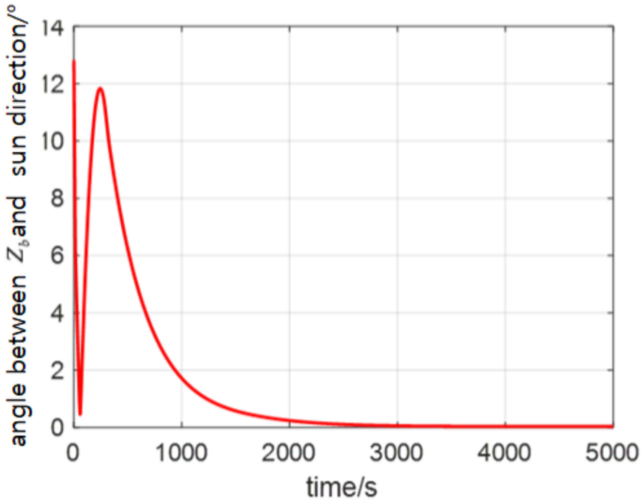

Figure 13. The time response of the angle between Z_b axis and sun direction.

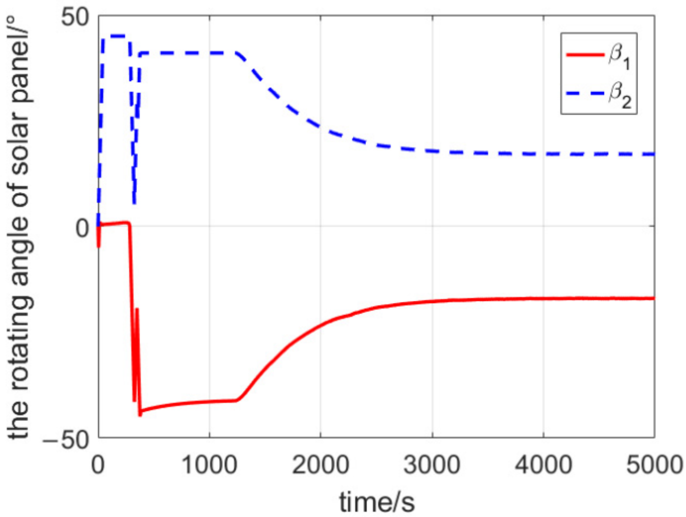

Figure 14. The time response of rotation angles of solar panels.

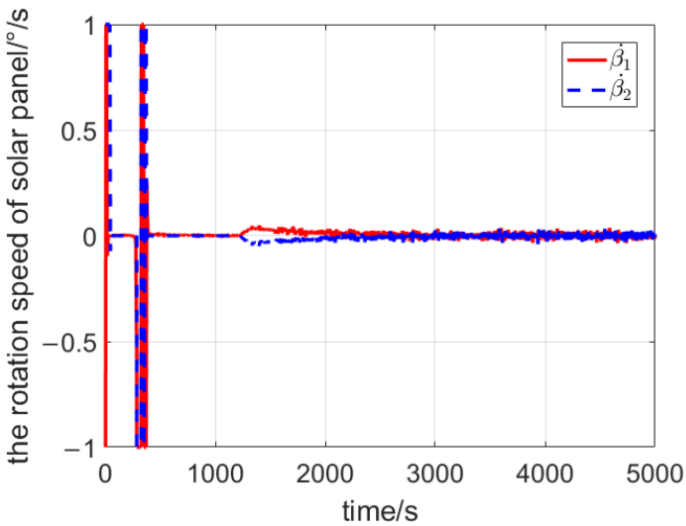

Figure 15. The time response of rotation speeds of solar panels.

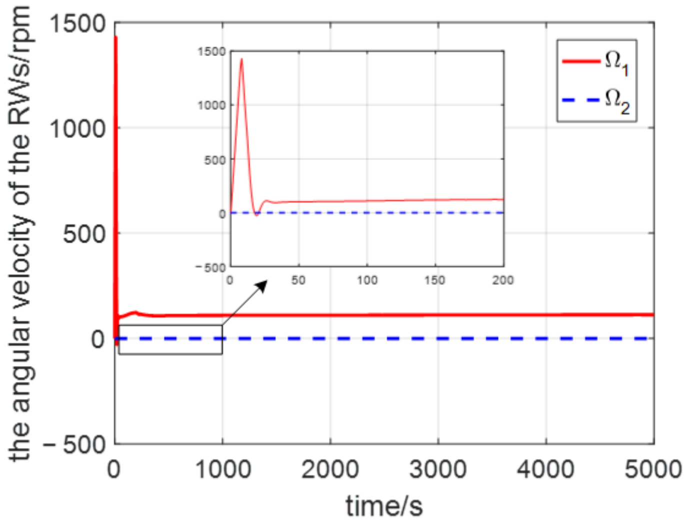

Figure 16. The time response of the angular velocity of RWs.

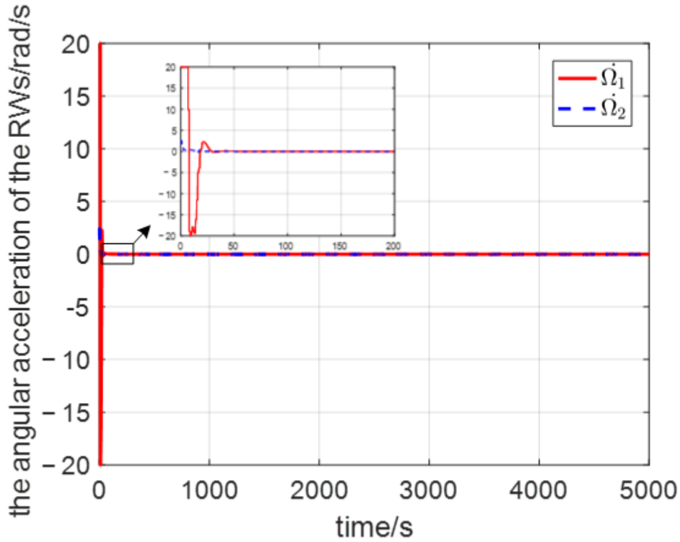

Figure 17. The time response of the angular acceleration of RWs.

According to Figures 10–12, the roll and pitch angles can be gradually stabilized, and the satellite eventually rotates around the yaw axis. Figure 13 shows that the angle between the Z_b axis and sun direction is gradually controlled to be zero, which means that the pointing stabilization control is realized. Figure 14 shows that the panels settle at the same rotation angle, and the SRP is zero with the same rotation angle. As the control system has reached a stable state, we can make the rotation speeds of the solar panels gradually become zero together to maintain better lighting conditions, as shown in Figure 15. The simulation in Figures 16 and 17 shows that the output of the reaction wheel on the Z axis is very small, and it proves that it is possible to achieve the inclined stabilization by choosing more suitable state variables with less control sources.

The above results show that the proposed dual-mode MPC can achieve three-axis stabilization control and pointing stabilization control, as well with the assistance of the solar radiation pressure.

5. Conclusions

In this paper, we consider a control problem for an under-actuated spacecraft with two reaction wheels. We assume that the solar panels of the under-actuated spacecraft can rotate within a certain angle so that the SRP torque can be tuned actively and used to assist the attitude control. In this case, the reliability and control performance of the under-actuated spacecraft, especially the deep space probes, can be greatly enhanced. We establish the model of the SRP torque acting on the spacecraft and take the rotation angles and rotation speeds of the panels as the state quantities and control quantities, respectively. Then, an integrated control scheme based on dual-mode MPC is proposed and the control quantities can be obtained directly. As this control method can resolve the constrained open-loop optimal control problem and ensure the robustness and stability of the closed-loop system, it has great value in engineering application. The numerical simulation results illustrate the validity of the control scheme proposed in this paper.

Author Contributions: Conceptualization, L.J.; methodology, L.J. and Y.L.; software, L.J. and Y.L.; validation, L.J. and Y.L.; formal analysis, L.J. and Y.L.; investigation, Y.L.; resources, L.J. and Y.L.; data curation, L.J. and Y.L.; writing—original draft preparation, Y.L.; writing—review and editing, Y.L.; visualization, Y.L.; supervision, L.J. and Y.L.; project administration, L.J.; funding acquisition, L.J. All authors have read and agreed to the published version of the manuscript.

Funding: This research was funded by The Fundamental Research Funds for the Central Universities, grant number YWF-19-BJ-J-272.

Data Availability Statement: Some or all data, models, or code that support the findings of this study are available from the corresponding author upon reasonable request.

Conflicts of Interest: The authors declare that they have no known competing financial interest or personal relationships that could have appeared to influence the work reported in this paper.

References

1. O'Donnell, J.R.; Andrews, S.; Ericsson-Jackson, A.; Flatley, T.; Ward, D.; Bay, P. Backup Attitude Control Algorithms for the MAP Spacecraft. In *Flight Mechanics Symposium, Proceeding of a Conference Sponsored and Held at NASA Goddard Space Flight Center*; Lynch, J.P., Ed.; NASA Goddard Space Flight Center: Greenbelt, MD, USA, 1999; pp. 391–405.
2. Starin, S.R.; O'Donnell, J.R. Development of a Two-Wheel Contingency Mode for the MAP Spacecraft. In Proceedings of the AIAA Guidance, Navigation, and Control Conference and Exhibit, Monterey, CA, USA, 5–8 August 2002; p. 4584.
3. Crouch, P. Spacecraft attitude control and stabilization: Applications of geometric control theory to rigid body models. *IEEE Trans. Autom. Control* **1984**, *29*, 321–331. [CrossRef]
4. Kruk, J.W.; Class, B.F.; Rovner, D.; Westphal, J.; Ake, T.B.; Moos, H.W.; Roberts, B.A.; Fisher, L. FUSE In-Orbit Attitude Control with Two Reaction Wheels and No Gyroscopes. In Proceedings of the Future EUV/UV and Visible Space Astrophysics Missions and Instrumentation, SPIE, Waikoloa, HI, USA, 2003; pp. 274–285.
5. Sahnow, D.J.; Kruk, J.W.; Ake, T.B.; Andersson, B.G.; Berman, A.; Blair, W.P.; Boyer, R.; Caplinger, J.; Calvani, H.; Civeit, T.; et al. Operations with the new FUSE observatory: Three-axis control with one reaction wheel. In Proceedings of the Space Telescopes and Instrumentation II: Ultraviolet to Gamma Ray, SPIE Astronomical Telescopes + Instrumentation, Orlando, FL, USA, 7 June 2006; p. 626602.
6. Thomas, T. Experiences with the BIRD Magnetic Coil System for Wheel Desaturation, Satellite Rate Damping and Attitude Control-the Concept of Virtual Wheel Systems. In Proceedings of the 5th Symposium on Small Satellites for Earth Observation, Berlin, Germany, 4–8 April 2005; pp. 361–368.
7. Krishnan, H.; McClamroch, H.; Reyhanoglu, M. Attitude Stabilization of a Rigid Spacecraft Using Two Momentum Wheel Actuators. *J. Guid. Control Dynamics.* **1995**, *18*, 256–263. [CrossRef]
8. Kim, S.; Kim, Y. Spin-Axis Stabilization of a Rigid Spacecraft Using Two Reaction Wheels. *J. Guid. Control Dyn.* **2001**, *24*, 1046–1049.
9. Horri, N.M.; Hodgart, S. Attitude Stabilization of an Underactuated Satellite Using Two Wheels. *IEEE Aerosp. Conf.* **2003**, *6*, 2629–2635.
10. Boyer, F.; Alamir, M. Further Results on the Controllability of a Two-wheeled Satellite. *J. Guid. Control Dyn.* **2007**, *30*, 611–619. [CrossRef]
11. Horri, N.M.; Palmer, P. Practical Implementation of Attitude-Control Algorithms for an Underactuated Satellite. *J. Guid. Control Dyn.* **2012**, *35*, 40–50.
12. Gui, H.C.; Jin, L.; Xu, S.J. Attitude Maneuver Control of a Two-Wheeled Spacecraft With Bounded Wheel Speeds. *Acta Astronautica.* **2013**, *88*, 98–107. [CrossRef]
13. Avanzini, G.; Zavoli, A.; Matteis, G.D.; Giulietti, F. Single Axis Pointing for Underactuated Spacecraft with a Residual Angular Momentum. *Aerosp. Sci. Technol.* **2022**, *124*, 107512. [CrossRef]
14. Ousaloo, S.H. Attitude Acquisition from an Arbitrary Tumbling State Using Two Skewed Reaction Wheels. *Aerosp. Sci. Technol.* **2018**, *72*, 84–94.

15. Han, C.Y.; Pechev, A.N. Time-Varing Nonlinear Designs for Underactuated Attitude Control with Two Reaction Wheels. In Proceedings of the 9th Biennial ASME Conference on Engineering Systems Design and Analysis, Haifa, Israel, 7–9 July 2008.
16. Nadafi, R.; Kabganian, M. Robust nonlinear attitude tracking control of an underactuated spacecraft under saturation and time-varying uncertainties. *Eur. J. Control* **2022**, *63*, 133–142. [CrossRef]
17. Siahpush, A.; Sexton, A. A Study for Semi-Passive Gravity Gradient Stabilization of Small Satellites. In Proceedings of the USU Conference on Small Satellites, Logan, UT, USA, 7–9 October 1987.
18. Avanzini, G.; Angelis, L.E.; Giulietti, F. Two-Timescale Magnetic Attitude Control of Low-Earth-Orbit Spacecraft. *Aerosp. Sci. Technol.* **2021**, *116*, 106884. [CrossRef]
19. Alger, M.; Ruiter, D.A. Magnetic Spacecraft Attitude Stabilization with Two Torquers. *Acta Astronautica.* **2022**, *192*, 157–167.g. [CrossRef]
20. Zeng, J.Q. Application of Aerodynamic Torque in Attitude Control of Ultra-low Orbit Satellite. Master's Thesis, Harbin Institute of Technology, Harbin, China, 2009.
21. Forbes, J.R.; Damaren, C.J. Geometric Approach to Spacecraft Attitude Control Using Magnetic and Mechanical Actuation. *J. Guid. Control Dyn.* **2010**, *33*, 590–595. [CrossRef]
22. Angelis, L.E.; Giulietti, F.; Ruiter, H.J.A.; Avanzini, G. Spacecraft Attitude Control Using Magnetic and Mechanical Actuation. *J. Guid. Control Dyn.* **2016**, *39*, 564–573. [CrossRef]
23. Ousaloo, S.H. Globally Asymptotic Three-axis Attitude Control for A Two-Wheeled Small Satellite. *Acta Astronaut.* **2019**, *157*, 17–28. [CrossRef]
24. Keshtkar, N.; Keshtkar, S.; Moreno, A.J.; Poznyak, A.; Kojima, H. LMI-Based Sliding Mode Control of an Underactuated Control Moment Gyroscope System. *IFAC Pap. Line* **2018**, *51*, 291–296. [CrossRef]
25. Lee, K.W.; Singh, S.N. Three-axis L1 adaptive attitude control of spacecraft using solar radiation pressure. *Proc. Inst. Mech. Eng. Part G J. Aerosp. Eng.* **2015**, *229*, 407–422. [CrossRef]
26. Lee, K.W.; Singh, S.N. A Higher-Order Sliding Mode Three-Axis Solar Pressure Satellite Attitude Control System. *J. Aerosp. Eng.* **2016**, *29*, 04015019. [CrossRef]
27. Cowen, R. The wheels come off Kepler. *Nature* **2013**, *497*, 417–418. [CrossRef]
28. Petersen, C.D.; Leve, F.; Flynn, M.; Kolmanovsky, I. Recovering Linear Controllability of an Underactuated Spacecraft by Exploiting Solar Radiation Pressure. *J. Guid. Control Dyn.* **2016**, *39*, 826–837. [CrossRef]
29. Thomas, S.; Michael, P.; Wie, B.; Murphy, D. AOCS performance and stability validation for large flexible solar sail spacecraft. American Institute of Aeronautics and Astronautics. In Proceedings of the 41st AIAA/ASME/SAE/ASEE Joint Propulsion Conference & Exhibit, Tucson, AZ, USA, 10–13 July 2005; p. 3926.
30. Wie, B.; Murphy, D. MicroPPT-based secondary/backup ACS for a 160-m, 450-kg solar sail spacecraft. American Institute of Aeronautics and Astronautics. In Proceedings of the 41st AIAA/ASME/SAE/ASEE Joint Propulsion Conference & Exhibit, Tucson, AZ, USA, 10–13 July 2005; p. 3724.
31. Funase, R.; Shirasawa, Y.; Mimasu, Y.; Mori, O.; Tsuda, Y.; Saiki, T.; Kawaguchi, J.I. On-orbit verification of fuel-free attitude control system for spinning solar sail utilizing solar radiation pressure. *Adv. Space Res.* **2011**, *48*, 1740–1746. [CrossRef]
32. Lei, J. Study on Attitude Dynamics and Control of Spacecraft Using Angular Momentum Exchange Devices. Ph.D. Thesis, Beihang University, Beijing, China, 2009.
33. Mclnnes, C.R. *Solar Sailing*; Springer London: London, UK, 1999.
34. Chen, H.; Allgöwer, F. A Quasi-Infinite Horizon Nonlinear Model Predictive Control Scheme with Guaranteed Stability. *Automatica* **1998**, *34*, 1205–1217. [CrossRef]
35. Mayne, D.Q.; Rawlings, J.B.; Rao, C.V.; Scokaert, P.O. Constrained model predictive control: Stability and optimality. *Automatica* **2000**, *36*, 789–814. [CrossRef]